Carbon Dioxide Photoreduction

International Edition: DOI: 10.1002/anie.201502319
German Edition: DOI: 10.1002/ange.201502319

Three-Dimensional Bimetal-Graphene-Semiconductor Coaxial Nanowire Arrays to Harness Charge Flow for the Photochemical Reduction of Carbon Dioxide**

Jungang Hou, Huijie Cheng, Osamu Takeda, and Hongmin Zhu**

Abstract: *The photochemical conversion of carbon dioxide provides a straightforward and effective strategy for the highly efficient production of solar fuels with high solar-light utilization efficiency. However, the high recombination rate of photoexcited electron–hole (e-h) pairs and the poor photostability have greatly limited their practical applications. Herein, a practical strategy is proposed to facilitate the separation of e-h pairs and enhance the photostability in a semiconductor by the use of a Schottky junction in a bimetal-graphene-semiconductor stack array. Importantly, Au-Cu nanoalloys (ca. 3 nm) supported on a 3D ultrathin graphene shell encapsulating a p-type Cu_2O coaxial nanowire array promotes the stable photochemical reduction of CO_2 to methanol by the synergetic catalytic effect of interfacial modulation and charge-transfer channel design. This work provides a promising lead for the development of practical catalysts for sustainable fuel synthesis.*

Carbon dioxide (CO_2), well-known as a greenhouse gas, the most important cause of global warming, is also an abundant carbon resource for fuels and organic materials.[1,2] It is a global issue for mankind to be achieved from the viewpoint of realizing a sustainable society through the fixation of atmospheric CO_2. The conversion of CO_2 into useful chemicals or fuels by artificial photosynthesis has been considered as one of the most promising and compelling approaches to solve both energy and environmental problems simultaneously.[3] Since Halmann discovered the photoelectrochemical reduction of CO_2, a growing interest in the development of photocatalysts has evolved.[4] Up to now, a great number of semiconductors (for example, TiO_2, WO_x, CdS), and titanates, niobates, tantalates, and gallates have been reported for the photoreduction of CO_2.[5] Thus, it is a topic of great interest with practical importance to develop visible-light-driven semiconductors for photochemical conversion of carbon dioxide.

Among the various semiconductors, p-type cuprous oxide (Cu_2O), with a suitable bandgap of 2.0 eV, is an attractive visible-light-driven photocatalyst owing to the appropriate conduction band that is negative of the hydrogen evolution potential, allowing Cu_2O to drive the water reduction reaction as photocathode.[6] Given the favorable attributes, Cu_2O is a promising candidate for the photochemical conversion of CO_2.[6,7] However, the practical photochemical application of Cu_2O is still limited by the charge separation and transfer capability and the poor stability owing to self-photocorrosion.[7] Therefore, it is a challenge to attempt to improve both the photochemical activity and stability of Cu_2O for CO_2 photoreduction.

It is well-known that nanostructured engineering can be employed to improve solar-driven photochemical performance.[8] Three-dimensional (3D) nanostructures are known as ideal building blocks for energy harvesting devices, providing an appealing platform, offering long optical paths for efficient light absorption, rapid electron–hole separation, and electrochemical reactions.[8] In particular, existing efforts have overwhelmingly focused on 3D Cu_2O photoelectrodes.[6,8] It is necessary to explore the photocatalytic activity of CO_2 reduction for 3D Cu_2O array.

To enhance the migration and separation of the photoexcited e-h pairs, a surface plasmon resonance of a metal–semiconductor junction across the space–charge region via a built-in electric field has offered a new opportunity to overcome the limited efficiency by: 1) extending light absorption to longer wavelengths; 2) increasing light scattering; and 3) exciting e-h pairs in the semiconductor by transferring the electrons between the metal and the semiconductor due to the Schottky barrier at the interface because the metals have a propagating surface plasmon resonance or localized surface plasmon resonance effect.[9] For instance, the presence of metals on the semiconductor has an enhancing effect over CO_2 conversion into hydrocarbons.[5a,b,10a] In particular, bimetals have attracted more attention for high catalytic efficiencies owing to the rapid harnessing of the charge flow in metal/semiconductor junctions.[5] Thus, a semiconductor–bimetal hybrid as a Schottky junction would expedite the separation of e-h pairs and promote more efficient redox reactions. However, maintaining long-time stability and high activity of the p-type semiconductor is still a great challenge.[6] Carbon materials have attracted tremendous research interest towards solar energy applications.[11]

[*] Dr. J. G. Hou, Dr. H. J. Cheng, Prof. H. M. Zhu
School of Metallurgical and Ecological Engineering
University of Science and Technology Beijing
Beijing 100083 (China)
E-mail: jhou@ustb.edu.cn
hzhu@material.tohoku.ac.jp
Dr. J. G. Hou, Dr. O. Takeda, Prof. H. M. Zhu
Tohoku University, Aramaki-Aza-Aoba, Aoba-ku
Sendai, 980-8579 (Japan)

[**] This work was supported by the National Science Foundation of China (No. 51472027), Beijing High School Youth Talent Plan (YETP0351), and National Basic Research Program of China (973 Program, No. 2013CB632404). J.G.H. thanks the Japan Society for the Promotion of Science (JSPS) for a fellowship at Tohoku University (Japan).

Supporting information for this article is available on the WWW under http://dx.doi.org/10.1002/anie.201502319.

For example, carbon quantum dots/Cu_2O heterostructures show efficient solar-light-driven conversion of CO_2 into methanol.[11b] The Cu_2O/reduced graphene oxide composites exhibit photocatalytic conversion of CO_2 into CO.[11c] Thus, there is a new platform for the construction of ultrathin graphene layers encapsulating a Cu_2O array for converting CO_2 into fuels. Despite the advances in this field, there is no report for the wide range of possibilities that simultaneous consideration of charge separation and stability by a novel bimetal–graphene–semiconductor stack design offers as an integrated array for the stable photochemical reduction of CO_2 to valuable fuels.

Herein, we develop such a novel bimetal–graphene–semiconductor stack design for solar-driven conversion of CO_2 into methanol in which 3D ultrathin graphene layers encapsulating a Cu_2O nanowire array supporting an optimized combination of Au-Cu nanoalloys (Au-Cu/graphene/Cu_2O) are used as the synergetic catalysts. Under visible-light irradiation, a methanol production rate of 18.80 $ppm\,cm^{-2}\,h^{-1}$ is achieved on the 3D Au-Cu/graphene/Cu_2O array. To be successful, the pivot improvement is the effectiveness of this novel photocatalyst owing to the following strategies: 1) a high surface area of 3D Cu_2O architectures consisting of nanowires that enhance the contact between charge carriers and surface species; 2) developing the ultrathin graphene layer encapsulating a Cu_2O nanowire array for efficient and stable photogenerated charge separation; and 3) achieving homogeneous bimetallic nanoalloys as a Schottky junction along the nanowire array to facilitate the photochemical reaction process.

The design and synthesis strategy of 3D Au-Cu/graphene/Cu_2O array is described in the Supporting Information (experimental details, Figures S1, S2). The Cu mesh was anodized in an alkali solution to form a 3D $Cu(OH)_2$/Cu mesh (Figure 1 a). After decoration, the Au-Cu/graphene/Cu_2O array on a copper mesh substrate was formed by a solution-phase approach. The XRD patterns of the $Cu(OH)_2$ and Cu_2O crystals exhibited a crystallized structure (Supporting Information, Figure S3), in agreement with the previous reports.[6] The SEM images (Figure 1 a–c) show that the Cu mesh substrate was uniformly covered with a dense layer of the $Cu(OH)_2$ nanowires. After annealing in Ar atmosphere and in situ reduction, the Au-Cu/graphene coupled Cu_2O/Cu mesh was obtained from the $Cu(OH)_2$/Cu mesh (Figure 1 d–f) in comparison of graphene-layer-protective Cu_2O/Cu mesh (Supporting Information, Figure S4). Figure 2 presents typical TEM images of the graphene/Cu_2O and Au-Cu/graphene/Cu_2O array, indicating that the ultrathin graphene layer with circa 3 nm was deposited on the surface of Cu_2O array and a large number of Au-Cu nanoalloys were uniformly dispersed on the support. Furthermore, the Au-Cu bimetallic nanoparticles with an average particle size of 3 nm was observed on the surface of the graphene layer (Figure 2). The high-resolution TEM images showed bimetal nanoparticles indexed as face-centered cubic (fcc) structures (Figure 2 e). The d-spacing values on Au-Cu nanoalloys was found to be 0.22 nm, which is different to that of Au ($d=$ 0.235 nm, Au (111), JCPDS 04-0784) and Cu ($d=0.208$ nm, Cu (111), JCPDS 04-0836).[5a] Based on the above-mentioned results of SEM/TEM images, the formation of the integrated 3D Au-Cu/graphene/Cu_2O array is confirmed. In particular, the composition of the Au-Cu nanoalloys were also determined by X-ray photoelectron spectra (XPS). The binding energy of Au $4f_{7/2}$ in the Au-Cu/graphene/Cu_2O array was 84.0 eV (Supporting Information, Figure S5), which was -0.4 lower than that in the Au/graphene/Cu_2O array (84.4 eV), whereas the binding energy of Cu $2p_{3/2}$ in the Cu/graphene/Cu_2O array was -0.2 eV higher than that in the Au-Cu/graphene/Cu_2O array (932.5 eV).[10] This shifting of binding energies of Au $4f_{7/2}$ and Cu $2p_{3/2}$ further confirm the formation of Au-Cu nanoalloys on the graphene/Cu_2O array.

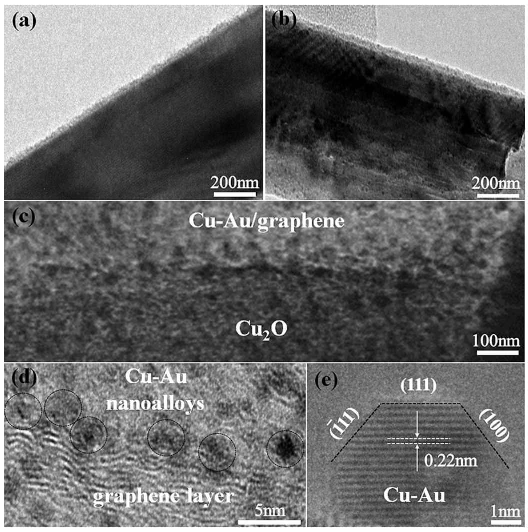

Figure 2. TEM and HRTEM images of the a) graphene/Cu_2O array and b)–e) Au-Cu/graphene/Cu_2O array.

To investigate in-depth the atomic structure of Au-Cu/graphene/Cu_2O array, XPS and FTIR and Raman spectroscopy were carried out (Figure 3). Figure 3 a displays the Cu 2p core-level spectrum. The Cu $2p_{3/2}$ and Cu $2p_{1/2}$ spin-orbital photoelectrons were located at binding energies of 932.5 eV and 952.4 eV, respectively.[6] After the combination of graphene, a notable decrease in oxygen content is clearly visible and the peak corresponding to the C−O bond has disappeared

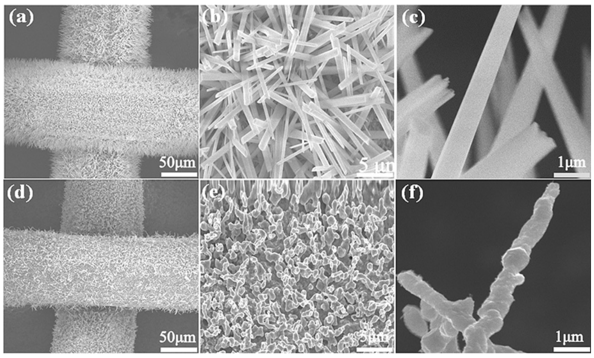

Figure 1. SEM images of a), b), c) $Cu(OH)_2$/Cu mesh and d), e), f) Au-Cu/graphene/Cu_2O/Cu mesh.

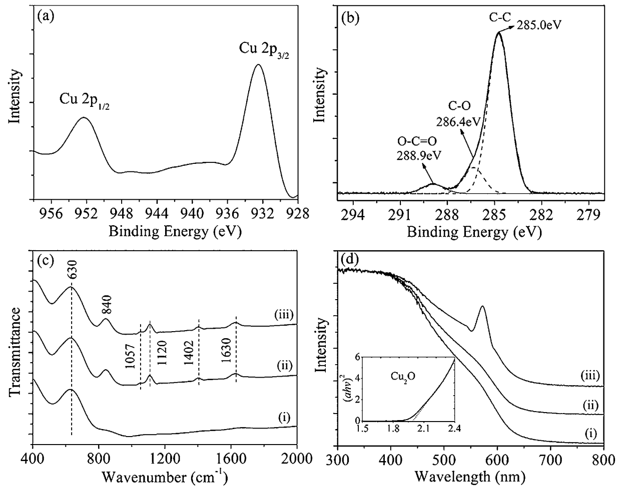

Figure 3. a), b) XPS spectra of the a) Cu 2p core level and b) C 1s core level of the Au-Cu/graphene/Cu_2O array. c) FTIR spectra and d) UV/Vis diffuse reflectance spectra of (i) Cu_2O, (ii) graphene/Cu_2O, and (iii) Au-Cu/graphene/Cu_2O arrays.

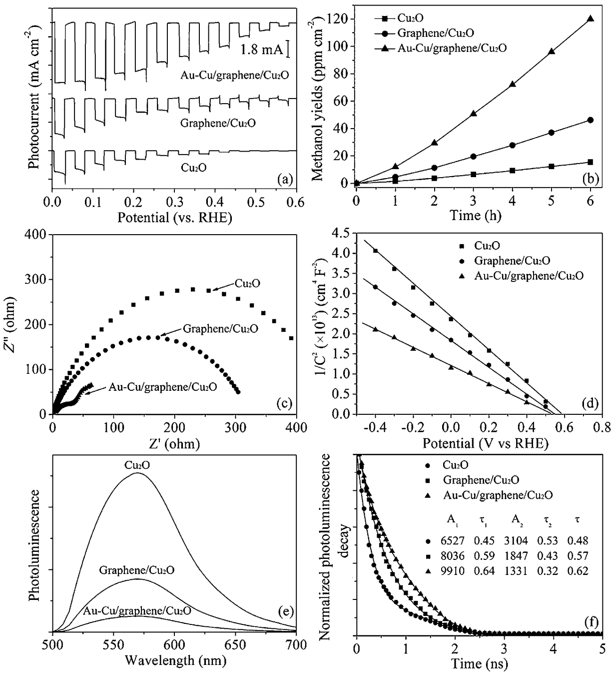

	A_1	τ_1	A_2	τ_2	τ
●	6527	0.45	3104	0.53	0.48
■	8036	0.59	1847	0.43	0.57
▲	9910	0.64	1331	0.32	0.62

Figure 4. a) Photoelectrochemical performance using Na_2SO_4 solution (pH 5) with potassium phosphate, b) yields of methanol as a function of time, c) Nyquist plots, d) Mott–Schottky plots, e) steady-state photoluminescence spectra (excitation: $\lambda = 420$ nm), and f) time-resolved photoluminescence decay curves (excitation: $\lambda = 420$ nm) for tunable Cu_2O, graphene/Cu_2O, and Au-Cu/graphene/Cu_2O arrays.

(Figure 3b).[6b,12] The oxygen loss mainly results from the loss of C−O (286.4 eV) and O−C=O (288.9 eV), indicating the partial removal of the oxygen-containing functional groups. The considerable deoxygenation by the hybrids will enhance the conductivity of system and achieve more effective preventing recombination during the catalytic process. Moreover, in Figure 3c, an obvious absorption band was observed at 630 cm^{-1} in the IR spectra of Cu_2O, which can be ascribed to the stretching vibration of the Cu−O band, confirming the formation of crystalline Cu_2O. In comparison, the characteristic bands of graphene are observed at 1057 cm^{-1} (alkoxy C−O stretching) and 1402 cm^{-1} (carboxyl O−H stretching).[11,12] The peak at 1120 cm^{-1} is ascribed to C−O stretching vibrations of carbonyl groups, and the broad absorption at 1630 cm^{-1} is related to H-O-H bending band of the adsorbed H_2O molecules or the in-plane vibrations of sp^2-hybridized C−C bonding.[12] To further confirm this point, the Raman spectra of various Cu_2O based arrays were conducted (Supporting Information, Figure S6). Thus, the analysis of XPS, FTIR, and Raman spectra indicate the presence of graphene in the hybrid arrays.

Diffuse-reflectance UV/Vis absorption spectra of various Cu_2O based arrays are presented in Figure 3d. After loading the graphene layer, the absorption ability of Cu_2O is relatively enhanced in the visible region owing to the scattering of the graphene to Cu_2O. In comparison to pure Au or Cu particles supported on a graphene/Cu_2O array (Supporting Information, Figure S7), a significant visible absorption peak around 570 nm for the Au-Cu/graphene/Cu_2O array was observed, which is due to the surface plasmonic resonance (SPR) absorption of the Au-Cu nanoalloys, in agreement with previous work,[5b,13] resulting into a significant enhancement of the light intensity around the visible region.

To demonstrate the superiority of the architecture, the photocurrent-density–potential (*J*–*V*) characteristics of a series of Cu_2O based photoelectrodes are shown in Figure 4a. All these *J*–*V* curves exhibit a cathodic photocurrent. The Au-Cu/graphene/Cu_2O array possesses a dramatic improvement in photocurrent after the coupling of graphene and Au-Cu nanoalloys, respectively. To confirm the CO_2 reduction, the long-term photoreduction of CO_2 and H_2O was performed for the Cu_2O-based arrays. The significant product of methanol was detected by GC analysis (Supporting Information, Figure S8). The yield of methanol from graphene/Cu_2O array is 46.29 ppm cm^{-2} after 6 h reaction, which is three times more than that of Cu_2O array (15.43 ppm cm^{-2}). Especially, the Au-Cu/graphene/Cu_2O array exhibited the highest methanol yield of 120.00 ppm cm^{-2}, which is higher 7.78 times than that of Cu_2O array after 6 h reaction. In comparison (Supporting Information, Figures S9–S11), after the linear fitting, the highest yield rate of 18.80 ppm cm^{-2} h^{-1} for the Au-Cu/graphene/Cu_2O array is achieved, which is considerably higher than the previous reports by use of Cu_2O-based catalysts.[7a,11b] However, the Au-Cu/Cu_2O array without the protection of graphene layer present the relatively lower methanol yield than that of the Au-Cu/graphene/Cu_2O array after 6 h reaction, indicating that the graphene layer plays a pivot role among the 3D architecture. Currently, the graphene/Cu_2O array decorated with Au, Cu and Au + Cu nanoalloys prepared by step-by-step deposition of metal on the support exhibit the much lower photocatalytic activities. In particular, the photocatalytic methanol yield of Au-Cu/graphene/Cu_2O array is higher than that of Au + Cu/graphene/Cu_2O array (Supporting Information, Figure S10), indicating that it is essential to reach the homogeneously mixed Au-Cu nanoalloys for the alloy effect. From the previous work, the electron densities on Au-Cu nanoalloys are much higher than the single Au and Cu nanoparticles owing to the alloy effect caused by the homogeneously mixed Au-Cu atoms.[5b,13] Moreover, the reverse transportation of the accumulated photogenerated electrons to the semiconductors was effectively restrained in the nanoalloys.[13c] Based on the above-mentioned results, the synergetic catalytic effect of graphene layer and Au-Cu nanoalloys by interfacial modulation and charge-transfer channels plays an important role upon the enhancement of photocatalytic reduction efficiency. Furthermore, after testing for five cycles, the yield rate of methanol from CO_2 conversion decreases from 18.80 to 17.30 ppm cm^{-2} h^{-1}, which is still 92% of its original activity (Supporting Information, Figures S11, S12), demonstrating that this combination of the nanoalloys and graphene layer on the Cu_2O array as the support opens a feasible approach over efficient and stable photocatalytic reduction conversion of CO_2 into methanol.

To understand the reasons of the enhanced CO_2 reduction yield, the further electrochemical and photoluminescence performances of the tunable Cu_2O-based arrays were conducted. As shown in Figure 4c, the Nyquist plots indicate that the charge transfer resistance of the system is prominently decreased by the usage of graphene and Au-Cu layer, given that the semicircle in a Nyquist plot at high frequencies is characteristic of the charge-transfer process and the diameter of the semicircle is estimated to be equal to the charge-transfer resistance.[14] Moreover, the slope of the linear part of the curves in the Mott–Schottky plot is negative, confirming a p-type semiconductor, which is in good agreement with the cathodic photocurrent density generated from the photocathodes (Figure 4d). The flat-band potential from the Mott–Schottky experiment of the Cu_2O nanowire array is about 0.58 V vs. RHE that is consistent with the onset potential of about 0.6 V vs. RHE for Cu_2O material.[13] Of note, the apparent flat-band potentials of the graphene/Cu_2O array and Au-Cu/graphene/Cu_2O array belong to 0.55–0.53 V vs. RHE due to the significant enhancement of the light intensity around the visible region owing to the scattering of the graphene to Cu_2O and the surface plasmonic resonance absorption of Au-Cu nanoalloys, and the Schottky junction effect and the efficient charge transport and separation in the integrated system. The slight modification shifts the flat band potentials negatively, resulting into a strengthened band bending at Cu_2O-based array/electrolyte interface that is profitable for transferring the photogenerated electrons to the surface. Accordingly, the value of carrier concentration estimated from the slope obtained from extrapolating the linear part of the curve to $1/C^2$ equals to zero on the potential axis for 3D Cu_2O, graphene/Cu_2O, and Au-Cu/graphene/Cu_2O arrays were 1.12×10^{19}, 1.38×10^{19} and 1.77×10^{19} cm^{-3}, respectively. In general, the increase in charge-carrier density is associated with increased electrical conductivity (σ) of the photoelectrode ($\sigma = en\mu$, where e is the electronic charge, n is the concentration of charge carriers, and μ is the mobility of the charge carriers).[15] Thus, the resistance of the system can be accordingly reduced, resulting into the increased mobility of the charge carriers is highly favorable for improving charge transport and charge separation processes.

The photoinduced electron transfer properties of the photocatalysts are potentially important for the photochemical CO_2 conversion.[7,14] The photoliminescence (PL) intensity and lifetime are useful probes of this property. The steady state PL spectra are shown in Figure 4e. After the introduction of graphene and Au-Cu nanoalloys, the PL intensities of the Au-Cu/graphene/Cu_2O array is markedly reduced to the lowest level in comparison of Cu_2O and graphene/Cu_2O arrays, demonstrating that the recombination of the photogenerated charges is significantly inhibited. In particular, Figure 4 f shows three representative time-resolved PL decays after pulsed excitation at $\lambda = 420$ nm. Obviously, the three curves present a rapid decay feature in nanosecond scale, which is in agreement with the reports.[6] After fitting the curves with exponential model (Supporting Information, Table S1), the lifetimes of as-prepared 3D Cu_2O, graphene/Cu_2O and Au-Cu/graphene/Cu_2O nanowire arrays were 0.48, 0.57 and 0.62 ns, respectively. Interestingly, the Au-Cu/graphene/Cu_2O array yields the longest decay time as compared with the intrinsic Cu_2O array and graphene/Cu_2O array, indicating an accelerated charge transfer mechanism induced by the modification of the graphene and Au-Cu alloys. This observation is indicative of a fast electron transfer via Cu_2O nanowire→graphene layer→Au-Cu nanoalloys. The accelerated charge transfer is bound to enhance the photocurrent and photoreduction yield.

The mechanism of CO_2 photoreduction is actually complex. This reduction process is proposed the multi-electron transfer instead of single electron transfer.[2] The Cu_2O is excited by visible light and produces electron–hole pairs; the electrons are consumed in CO_2 reduction to methanol on the Cu_2O surface.[7] After coupling the protective layer, with a lower activation potential of graphene, the role of ultrathin graphene layer as an electron acceptor that can extract electrons from Cu_2O retards the possible reduction of Cu_2O efficiency and improves photostability of the photocatalyst significantly.[11b] Since the simultaneous introduction of graphene and Au-Cu nanoalloys, the mechanism of efficient visible-light-driven reduction of CO_2 to methanol was proposed: 1) When 3D Au-Cu/graphene/Cu_2O nanowire array captured solar illumination, Cu_2O simultaneously generated photoelectrons and holes; 2) the photogenerated electrons migrated to the graphene layer from the conduction band (CB) of Cu_2O owing to the introduction of graphene as an electron conductive platform, the work function of which is less negative than the CB of Cu_2O;[16] 3) the formation of Schottky junction in 3D Au-Cu/graphene/Cu_2O system results into the further migration of electrons from graphene to Au-Cu nanoalloys due to the surface plasmonic resonance effect under visible-light irradiation. The electron–hole pairs are readily separated under the influence of the surface potential and their distance to travel to the surface of Cu_2O, where they can react with water in a photochemical reaction, is shortened. Meanwhile, the Fermi level of p-type Cu_2O is located at a more negative level than that of Au or Cu metal.[6,17] Combined with the formation of Schottky junction with the surface plasmon resonance effect, the band structure of Au-Cu/graphene/Cu_2O is shown in Figure 5. In particulat, the Au-Cu/graphene/Cu_2O system generates an electromagnetic field that promotes the migration of electrons through the harness charge flow of Cu_2O nanowire array→graphene layer→Au-

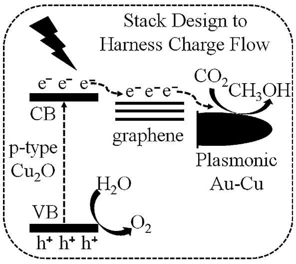

Figure 5. Diagram of the CO_2 photoreduction mechanism for the Au-Cu/graphene/Cu_2O array.

Cu nanoalloys. From Figure 4, these results demonstrate that Au-Cu nanoalloys can efficiently store the electrons photogenerated in the semiconductor system, which become readily available to drive the multi-electron CO_2 reduction process. Currently, the oxidation reaction happens on the surface of Cu_2O (Supporting Information, Figure S13). The existence of ultrathin graphene layer in particular plays a pivot role on the stability of p-type Cu_2O nanowire array. Therefore, the synergetic catalytic effect through the interfacial modulation and charge-transfer channels design by use of the integration of graphene layer and Au-Cu nanoalloys play a pivot role upon the enhancement of practically photocatalystic reduction of CO_2 into sustainable fuels.

In summary, we have successfully demonstrated the 3D Au-Cu/graphene/Cu_2O integrated system for highly selective methanol production from CO_2 directly. Our newly developed photocatalyst is capable of harvesting sufficient visible light for carrying out the multi-electron reduction of CO_2 to methanol upon integration with a sequentially coupled ultrathin graphene layer and Au-Cu nanoalloys. To the best of our knowledge, this is the first report on CO_2 fixation exclusively as methanol by a bimetal/graphene/semiconductor integrated system. On the whole, our approach provides an appealing strategy for selective methanol production from CO_2 by the use of inexpensive and abundantly available solar energy.

Keywords: carbon dioxide · Cu_2O nanowire arrays · gold · graphene layers · photoreduction

How to cite: *Angew. Chem. Int. Ed.* **2015**, *54*, 8480–8484
Angew. Chem. **2015**, *127*, 8600–8604

[1] M. Pera-Titus, *Chem. Rev.* **2014**, *114*, 1413.
[2] A. J. Morris, G. J. Meyer, E. Fujita, *Acc. Chem. Res.* **2009**, *42*, 1983.
[3] X. Zhang, F. Han, B. Shi, S. Farsinezhad, G. P. Dechaine, K. Shankar, *Angew. Chem. Int. Ed.* **2012**, *51*, 11778; *Angew. Chem.* **2012**, *124*, 11948.
[4] M. Halmann, *Nature* **1978**, *275*, 115.
[5] a) Ş. Neaţu, J. A. Maciá-Agulló, P. Concepción, H. Garcia, *J. Am. Chem. Soc.* **2014**, *136*, 15969; b) Q. Kang, T. Wang, P. Li, L. Q. Liu, K. Chang, M. Li, J. H. Ye, *Angew. Chem. Int. Ed.* **2015**, *54*, 841; *Angew. Chem.* **2015**, *127*, 855; c) G. C. Xi, S. X. Ouyang, P. Li, J. H. Ye, Q. Ma, N. Su, H. Bai, C. Wang, *Angew. Chem. Int. Ed.* **2012**, *51*, 2395; *Angew. Chem.* **2012**, *124*, 2445; d) Y. S. Chaudhary, T. W. Woolerton, C. S. Allen, J. H. Warner, E. Pierce, S. W. Ragsdale, F. A. Armstrong, *Chem. Commun.* **2012**, *48*, 58; e) K. Xie, N. Umezawa, N. Zhang, P. Reunchan, Y. Zhang, J. H. Ye, *Energy Environ. Sci.* **2011**, *4*, 4211; f) H. Zhou, J. J. Guo, P. Li, T. X. Fan, D. Zhang, J. H. Ye, *Sci. Rep.* **2013**, *3*, 1667; g) K. Iizuka, T. Wato, Y. Miseki, K. Saito, A. Kudo, *J. Am. Chem. Soc.* **2011**, *133*, 20863; h) S. C. Yan, S. X. Ouyang, J. Gao, M. Yang, J. Y. Feng, X. X. Fan, L. J. Wan, Z. S. Li, J. H. Ye, Y. Zhou, Z. G. Zou, *Angew. Chem. Int. Ed.* **2010**, *49*, 6400; *Angew. Chem.* **2010**, *122*, 6544.
[6] a) M. A. Mahmoud, W. Qian, M. A. El-Sayed, *Nano Lett.* **2011**, *11*, 3285; b) Z. H. Zhang, R. Dua, L. B. Zhang, H. B. Zhu, H. N. Zhang, P. Wang, *ACS Nano* **2013**, *7*, 1709; c) A. Paracchino, V. Laporte, K. Sivula, M. Grätzel, E. Thimsen, *Nat. Mater.* **2011**, *10*, 456; d) S. I. In, D. D. Vaughn II, R. E. Schaak, *Angew. Chem. Int. Ed.* **2012**, *51*, 3915; *Angew. Chem.* **2012**, *124*, 3981; e) C. G. Morales-Guio, S. D. Tilley, H. Vrubel, M. Grätzel, X. L. Hu, *Nat. Commun.* **2014**, *5*, 3059.
[7] a) H. Li, Y. Lei, Y. Huang, Y. Fang, Y. Xu, L. Zhu, X. Li, *J. Natural Gas Chem.* **2011**, *20*, 145; b) C. W. Li, M. W. Kanan, *J. Am. Chem. Soc.* **2012**, *134*, 7231.
[8] a) A. I. Hochbaum, P. D. Yang, *Chem. Rev.* **2010**, *110*, 527; b) J. Shi, Y. Hara, C. L. Sun, M. A. Anderson, X. D. Wang, *Nano Lett.* **2011**, *11*, 3413; c) A. Kargar, Y. Jing, S. J. Kim, C. T. Riley, X. Q. Pan, D. L. Wang, *ACS Nano* **2013**, *7*, 11112; d) A. A. Dubale, W. N. Su, A. G. Tamirat, C. J. Pan, B. A. Aragaw, H. M. Chen, C. H. Chen, B. J. Hwang, *J. Mater. Chem. A* **2014**, *2*, 18383; e) J. G. Hou, C. Yang, H. J. Cheng, S. Q. Jiao, O. Takeda, H. M. Zhu, *Energy Environ. Sci.* **2014**, *7*, 3758; f) J. G. Hou, Z. Wang, C. Yang, H. J. Cheng, S. Q. Jiao, H. M. Zhu, *Energy Environ. Sci.* **2013**, *6*, 3322; g) J. G. Hou, C. Yang, H. J. Cheng, O. Takeda, H. M. Zhu, *Energy Environ. Sci.* **2015**, *8*, 1348.
[9] a) A. L. Linsebigler, G. Lu, J. T. Yates, Jr., *Chem. Rev.* **1995**, *95*, 735; b) C. Gomes Silva, R. Juárez, T. Marino, R. Molinari, H. García, *J. Am. Chem. Soc.* **2011**, *133*, 595; c) X. M. Zhang, Y. L. Chen, R. S. Liu, D. P. Tsai, *Rep. Prog. Phys.* **2013**, *76*, 046401.
[10] a) W. N. Wang, W. J. An, B. Ramalingam, S. Mukherjee, D. M. Niedzwiedzki, S. Gangopadhyay, P. Biswas, *J. Am. Chem. Soc.* **2012**, *134*, 11276; b) Y. Shiraishi, H. Sakamoto, Y. Sugano, S. Ichikawa, T. Hirai, *ACS Nano* **2013**, *7*, 9287; c) X. Y. Wan, C. M. Zhou, J. S. Chen, W. P. Deng, Q. H. Zhang, Y. H. Yang, Y. Wang, *ACS Catal.* **2014**, *4*, 2175.
[11] a) Q. J. Xiang, J. G. Yu, M. Jaroniec, *Chem. Soc. Rev.* **2012**, *41*, 782; b) H. D. Li, X. Y. Zhang, D. R. MacFarlane, *Adv. Energy Mater.* **2014**, *140*, 1077; c) X. Q. An, K. F. Li, J. W. Tang, *ChemSusChem* **2014**, *7*, 1086.
[12] Q. Li, B. D. Guo, J. G. Yu, J. R. Ran, B. H. Zhang, H. J. Yan, J. R. Gong, *J. Am. Chem. Soc.* **2011**, *133*, 10878.
[13] a) Z. H. Zhang, L. B. Zhang, M. N. Hedhili, H. N. Zhang, P. Wang, *Nano Lett.* **2013**, *13*, 14; b) Y. Sugano, Y. Shiraishi, D. Tsukamoto, S. Ichikawa, S. Tanaka, T. Hirai, *Angew. Chem. Int. Ed.* **2013**, *52*, 5295; *Angew. Chem.* **2013**, *125*, 5403; c) R. Su, R. Tiruvalam, A. J. Logsdail, Q. He, C. A. Downing, M. T. Jensen, N. Dimitratos, L. Kesavan, P. P. Wells, R. Bechstein, *ACS Nano* **2014**, *8*, 3490.
[14] a) S. Bai, J. Ge, L. Wang, M. Gong, M. Deng, Q. Kong, L. Song, J. Jiang, Q. Zhang, Y. Luo, Y. Xie, Y. Xiong, *Adv. Mater.* **2014**, *26*, 5689; b) Y. Ma, H. Xu, Y. Zeng, C. L. Ho, C. H. Chui, Q. Zhao, W. Huang, W. Y. Wong, *J. Mater. Chem. C* **2015**, *3*, 66.
[15] M. Zhou, J. Bao, Y. Xu, J. J. Zhang, J. F. Xie, M. L. Guan, C. L. Wang, L. Y. Wen, Y. Lei, Y. Xie, *ACS Nano* **2014**, *8*, 7088.
[16] a) J. Zhang, J. G. Yu, M. Jaroniec, J. R. Gong, *Nano Lett.* **2012**, *12*, 4584; b) C. Han, Z. Chen, N. Zhang, J. C. Colmenares, Y. J. Xu, *Adv. Funct. Mater.* **2015**, *25*, 221.
[17] F. Shao, J. Sun, L. Gao, J. Q. Luo, Y. Q. Liu, S. W. Yang, *Adv. Funct. Mater.* **2012**, *22*, 3907.

Received: March 12, 2015
Revised: April 13, 2015
Published online: June 9, 2015

